

Neutrino masses, dark matter and leptogenesis with $U(1)_{B-L}$ gauge symmetry

Chao-Qiang Geng^{1,2,3,*} and Hiroshi Okada^{2,†}

¹*School of Physics and Information Engineering,
Shanxi Normal University, Linfen 041004, China*

²*Physics Division, National Center for Theoretical Sciences, Hsinchu, Taiwan 300*

³*Department of Physics, National Tsing Hua University, Hsinchu, Taiwan 300*

(Dated: February 19, 2018)

Abstract

We propose a model with an $U(1)_{B-L}$ gauge symmetry, in which small neutrino masses, dark matter and the matter-antimatter asymmetry in the Universe can be simultaneously explained. In particular, the neutrino masses are generated radiatively, while the matter-antimatter asymmetry is led by the leptogenesis mechanism, at TeV scale. We also explore allowed regions of the model parameters and discuss some phenomenological effects, including lepton flavor violating processes.

*Electronic address: geng@phys.nthu.edu.tw

†Electronic address: macokada3hiroshi@cts.nthu.edu.tw

I. INTRODUCTION

Radiative neutrino mass generation is one of the most promising candidates to naturally explain the small mass scales of active neutrinos. Some models to realize this type of the approach can also accommodate dark matter (DM). Normally, when one considers the DM candidate in a theory, an additional symmetry such as Z_2 is imposed in order to stabilize it. The representative model has been shown in ref. [1]. In recent years, a lot of applications have been presented in the literature. In particular, a model in ref. [2] with introducing $Z_2 \times Z_2$ symmetry and two inert isospin doublet bosons was proposed to understand the cosmic ray anomaly [3] by a decaying fermionic DM. In this model, the Baryon Asymmetry of the Universe (BAU) is understood via the leptogenesis mechanism within the TeV scale.

Our paper extends the study in ref. [2] by having a gauged $U(1)_{B-L}$ symmetry instead of $Z_2 \times Z_2$, in which three right-handed neutrinos are naturally introduced as a usual model with the $U(1)_{B-L}$ symmetry. However, their charge assignments are taken with a very unique manner, *i.e.* $-4, -4$ and 5 for three right-handed neutrinos [4, 5], respectively.¹ It suggests that the first two right-handed neutrinos can contribute to the active neutrinos with masses, while the third right-handed one can be a good DM candidate, even though two kinds of new bosons with nonzero $B - L$ charges have to be added to give the masses of right-handed neutrinos. As a result, the stabilized symmetry of DM (Z_2) is induced as a remnant symmetry after the spontaneous symmetry breaking (SSB) of $U(1)_{B-L}$.²

This paper is organized as follows. In Sec. II, we first set up our model. We then discuss the Higgs sector, the active neutrinos, leptogenesis, lepton flavor violating (LFV) processes and dark matter. In Sec. III, we give the numerical analysis to explore the allowed parameter space of the model. We conclude in Sec. IV.

¹ Several applications along this ideas can be found in refs. [6–9]

² A $U(1)_{B-L}$ gauge symmetry is sometimes embedded in larger groups such as $SU(2)_L \times SU(2)_R$, $SU(4)$, $SU(5)$, and $SO(10)$. See, *e.g.*, refs. [10, 11].

II. MODEL SETUP AND PHENOMENOLOGIES

First of all, we impose an additional $U(1)_{B-L}$ gauge symmetry and add three right-handed neutral fermions $N_{R_i} (i = 1, 2, 3)$ to the standard model (SM), where the right-handed neutrinos have $U(1)_{B-L}$ charges of -4 , -4 and 5 , respectively. Consequently, all the anomalies to be considered are the triangular $U(1)_{B-L}^3$ and mixed gauged-gravity $U(1)_{B-L}$ ones, which are found to be zero [4, 5], due to the uniqueness of the charge assignments in the SM [12]. We also introduce φ_8 and φ_{10} with nonzero vacuum expectation values (VEVs) after the SSB of $U(1)_{B-L}$. As a result, three right-handed neutral fermions acquire nonzero Majorana masses. Note here that one is still unable to understand active neutrino masses due to the absence of the Yukawa term $\bar{L}_L \tilde{H} N_R$. To solve this problem, we place $SU(2)_L$ doublet bosons ζ and η with nonzero $U(1)_{B-L}$ charges, so that neutrino masses are radiatively generated at one-loop level. Here, ζ is expected to be inert, whereas η is not. Also the stability of DM is assured by a remnant Z_2 symmetry after the SSB of $U(1)_{B-L}$. Field contents and their assignments for fermions and bosons are given in Table I and II, respectively. The renormalizable Lagrangian for the lepton sector and Higgs potential are

TABLE I: Field contents of fermions and their charge assignments under $SU(3)_C \times SU(2)_L \times U(1)_Y \times U(1)_{B-L}$, where $i = 1, 2$.

Fermions	Q_L	u_R	d_R	L_L	e_R	N_{R_i}	N_{R_3}
$SU(3)_C$	3	3	3	1	1	1	1
$SU(2)_L$	2	1	1	2	1	1	1
$U(1)_Y$	$\frac{1}{6}$	$\frac{2}{3}$	$-\frac{1}{3}$	$-\frac{1}{2}$	-1	0	0
$U(1)_{B-L}$	$\frac{1}{3}$	$\frac{1}{3}$	$\frac{1}{3}$	-1	-1	-4	5

given by

$$-\mathcal{L}_L = y_{\ell_a} \bar{L}_{L_a} e_{R_a} H + (y_\zeta)_{ai} \bar{L}_{L_a} \tilde{\zeta} N_{R_i} + \frac{y_{N_i}}{2} \bar{N}_{R_i}^C N_{R_i} \varphi_8 + \frac{y_{N_3}}{2} \bar{N}_{R_3}^C N_{R_3} \varphi_{10}^* + \text{h.c.}, \quad (1)$$

$$\begin{aligned} V = & \mu_H^2 |H|^2 + \mu_\eta^2 |\eta|^2 + \mu_\zeta^2 |\zeta|^2 + \mu_{\varphi_8}^2 |\varphi_8|^2 + \mu_{\varphi_{10}}^2 |\varphi_{10}|^2 + \frac{\lambda_0}{2} [(H^\dagger \zeta)(\eta^\dagger \zeta) + \text{h.c.}] \\ & + \frac{\lambda_H}{4} |H|^4 + \frac{\lambda_\eta}{4} |\eta|^4 + \frac{\lambda_\zeta}{4} |\zeta|^4 + \frac{\lambda_{\varphi_8}}{4} |\varphi_8|^4 + \frac{\lambda_{\varphi_{10}}}{4} |\varphi_{10}|^4 + \lambda_{H\eta} |H|^2 |\eta|^2 + \lambda'_{H\eta} |H^\dagger \eta|^2 \\ & + \lambda_{H\zeta} |H|^2 |\zeta|^2 + \lambda'_{H\zeta} |H^\dagger \zeta|^2 + \lambda_{H\varphi_8} |H|^2 |\varphi_8|^2 + \lambda_{H\varphi_{10}} |H|^2 |\varphi_{10}|^2 + \lambda_{\eta\zeta} |\eta|^2 |\zeta|^2 + \lambda'_{\eta\zeta} |\eta^\dagger \zeta|^2 \\ & + \lambda_{\eta\varphi_8} |\eta|^2 |\varphi_8|^2 + \lambda_{\eta\varphi_{10}} |\eta|^2 |\varphi_{10}|^2 + \lambda_{\zeta\varphi_8} |\zeta|^2 |\varphi_8|^2 + \lambda_{\zeta\varphi_{10}} |\zeta|^2 |\varphi_{10}|^2 + \lambda_{\varphi_8\varphi_{10}} |\varphi_8|^2 |\varphi_{10}|^2, \end{aligned} \quad (2)$$

respectively, where $\tilde{\zeta} \equiv (i\sigma_2)\zeta^*$ with σ_2 being the second Pauli matrix, and $a(i)$ runs over 1 to 3(2).

In the *scalar sector*, the scalar fields are parameterized as

$$H = \begin{bmatrix} w^+ \\ \frac{v+h+iz}{\sqrt{2}} \end{bmatrix}, \quad \eta = \begin{bmatrix} \eta^+ \\ \frac{v_\eta + \eta_R + i\eta_I}{\sqrt{2}} \end{bmatrix}, \quad \zeta = \begin{bmatrix} \zeta^+ \\ \frac{\zeta_R + i\zeta_I}{\sqrt{2}} \end{bmatrix}, \quad \varphi_i = \frac{v_{\varphi_i} + \varphi_{R_i} + iz_{\varphi_i}}{\sqrt{2}}, \quad (i = 8, 10), \quad (3)$$

where $\sqrt{v^2 + v_\eta^2} \approx 246$ GeV, each of the lightest states (=massless states) of (w^\pm, η^\pm) and (z, η_I) , and $(z_{\varphi_8}, z_{\varphi_{10}})$ is absorbed by the SM gauge bosons of W^\pm and Z , and the $B - L$ gauge boson of Z' , induced after the SSB. Inserting tadpole conditions, the singly-charged mass matrix with 2 by 2 in the basis of $(w^\pm, \eta^\pm)^T$ is defined by M_C , which is diagonalized by the orthogonal matrix O_C as $m_{H_i^\pm}^2 = O_C M_C^2 O_C^T$, ($i = 1, 2$) with $H_i^\pm (m_{H_i^\pm})$ the mass

TABLE II: Field contents of bosons and their charge assignments under $SU(3)_C \times SU(2)_L \times U(1)_Y \times U(1)_{B-L}$.

Bosons	H	ζ	η	φ_8	φ_{10}
$SU(3)_C$	1	1	1	1	1
$SU(2)_L$	2	2	2	1	1
$U(1)_Y$	$\frac{1}{2}$	$\frac{1}{2}$	$\frac{1}{2}$	0	0
$U(1)_{B-L}$	0	-3	-6	8	10

eigenstates (eigenvalues), where

$$M_C^2 = \frac{\lambda'_{H\eta}}{2} \begin{bmatrix} v_\eta^2 & -vv_\eta \\ -vv_\eta & v^2 \end{bmatrix}, \quad O_C = \begin{bmatrix} \frac{v}{\sqrt{v^2+v_\eta^2}} & \frac{v_\eta}{\sqrt{v^2+v_\eta^2}} \\ -\frac{v_\eta}{\sqrt{v^2+v_\eta^2}} & \frac{v}{\sqrt{v^2+v_\eta^2}} \end{bmatrix}, \quad m_{H_i^\pm}^2 = \begin{bmatrix} 0 & 0 \\ 0 & \frac{\lambda'_{H\eta}}{2}(v^2 + v_\eta^2) \end{bmatrix}. \quad (4)$$

Therefore, the structure of (w^\pm, η^\pm) is same as one of the two Higgs doublet models [13]. In the same way as the singly-charged case, the CP even matrix with 4 by 4 in the basis of $(h, \eta_R, \varphi_{R8}, \varphi_{R10})^T$ is defined by M_R , which is diagonalized by the orthogonal matrix O_R as $m_{h_i}^2 = O_R M_R^2 O_R^T$, ($i = 1, 2, \dots, 4$) with $h_i(m_{h_i})$ the mass eigenstates (eigenvalues). Furthermore, the SM Higgs is defined by $h_{SM} \equiv h_1$ with $m_{h_{SM}} \equiv m_{h_1} = 125$ GeV. The concrete form of M_R is given by

$$M_R^2 \equiv \begin{bmatrix} \frac{v^2 \lambda_H}{2} & vv_\eta(\lambda_{H\eta} + \lambda'_{H\eta}) & vv_{\varphi_8} \lambda_{H\varphi_8} & vv_{\varphi_{10}} \lambda_{H\varphi_{10}} \\ vv_\eta(\lambda_{H\eta} + \lambda'_{H\eta}) & \frac{v_\eta^2 \lambda_\eta}{2} & v_\eta v_{\varphi_8} \lambda_{\eta\varphi_8} & v_\eta v_{\varphi_{10}} \lambda_{\eta\varphi_{10}} \\ vv_{\varphi_8} \lambda_{H\varphi_8} & v_\eta v_{\varphi_8} \lambda_{\eta\varphi_8} & \frac{v_{\varphi_8}^2 \lambda_{\varphi_8}}{2} & v_{\varphi_8} v_{\varphi_{10}} \lambda_{\varphi_8\varphi_{10}} \\ vv_{\varphi_{10}} \lambda_{H\varphi_{10}} & v_\eta v_{\varphi_{10}} \lambda_{\eta\varphi_{10}} & v_{\varphi_8} v_{\varphi_{10}} \lambda_{\varphi_8\varphi_{10}} & \frac{v_{\varphi_{10}}^2 \lambda_{\varphi_{10}}}{2} \end{bmatrix}, \quad (5)$$

where the O_R and m_{h_i} are numerically obtained. In the inert sector, the mass eigenstates of $\zeta_{R(I)}$ and ζ^\pm are given by [14]

$$m_{\zeta_R}^2 = M_\zeta^2 + \frac{1}{2} \lambda_0 vv_\eta, \quad m_{\zeta_I}^2 = M_\zeta^2 - \frac{1}{2} \lambda_0 vv_\eta, \quad m_{\zeta^\pm}^2 = M_\zeta^2 - \frac{1}{2} \lambda'_{\eta\zeta} v_\eta^2, \quad (6)$$

$$M_\zeta^2 = \mu_\zeta^2 + \frac{1}{2} [\lambda_{\zeta\varphi_8} v_{\varphi_8}^2 + \lambda_{\zeta\varphi_{10}} v_{\varphi_{10}}^2 + (\lambda_{\eta\zeta} + \lambda'_{\eta\zeta}) v_\eta^2]. \quad (7)$$

Here, we will briefly discuss the breaking scale of $U(1)_{B-L}$. Because of our large numbers of $B-L$ charge assignments for bosons φ_8 and φ_{10} in Table II, our theory can really be within the TeV scale, where these bosons cause the SSB of $U(1)_{B-L}$ in order to give masses of the right-handed neutrinos with $B-L$ charges $(-4, -4, 5)$. The breaking scale could be evaluated by the mass of the $B-L$ gauge boson. Once we fix the gauge coupling of $B-L$ (g') to be $O(1)$, its typical mass is greater than 6.9 TeV from the LEP constraint [25]. On the other hand, its theoretical mass in our model can be given by $m_{Z'} = g' \sqrt{(8v_{\varphi_8})^2 + (10v_{\varphi_{10}})^2}$. Even assuming $v_{\varphi_8} \gg v_{\varphi_{10}}$, the typical breaking scale of $B-L$ can be less than 1 TeV.

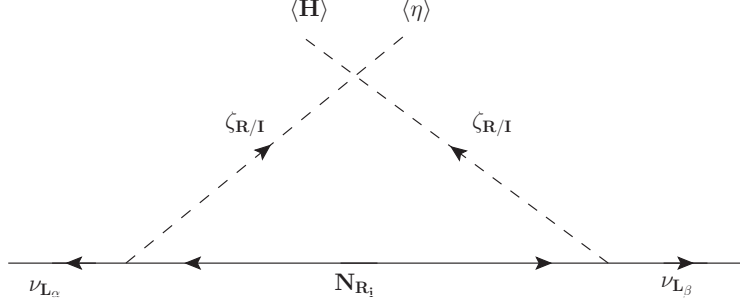


FIG. 1: One loop diagram which induces neutrino masses.

A. Neutrino masses

Since y_ℓ and y_N can be diagonal without loss of generality in Eq. (1), we define $m_{\ell_a} = y_{\ell_a} v / \sqrt{2}$ ($a = e, \mu, \tau$) $M_{N_i} = y_{N_i} v_{\varphi_8} / \sqrt{2}$ ($i = 1, 2$) after the electroweak and $U(1)_{B-L}$ symmetry breakings, where m_ℓ and M_N are respectively the masses of charged-leptons and right-handed neutrinos. The neutrino mass matrix is induced at one-loop level as shown in Fig. 1, and its form is given by [1]

$$(\mathcal{M}_\nu)_{\alpha\beta} = \frac{1}{16\pi^2} \sum_{i=1,2} (y_\zeta)_{\alpha i} (y_\zeta^T)_{i\beta} M_{N_i} \left(\frac{m_{\zeta_R}^2}{m_{\zeta_R}^2 - M_{N_i}^2} \ln \left[\frac{m_{\zeta_R}^2}{M_{N_i}^2} \right] - \frac{m_{\zeta_I}^2}{m_{\zeta_I}^2 - M_{N_i}^2} \ln \left[\frac{m_{\zeta_I}^2}{M_{N_i}^2} \right] \right). \quad (8)$$

We note that the Casas-Ibarra parametrization is a convenient method to achieve the numerical analysis [17]. Once we define $m_\nu \equiv U_{MNS} \mathcal{M}_\nu U_{MNS}^T$, y_ζ can be replaced by observables with several arbitral parameters given by

$$y_\zeta = U_{MNS}^\dagger m_\nu^{1/2} O R^{-1/2},$$

$$R \equiv \frac{1}{16\pi^2} \sum_{i=1,2} M_{N_i} \left(\frac{m_{\zeta_R}^2}{m_{\zeta_R}^2 - M_{N_i}^2} \ln \left[\frac{m_{\zeta_R}^2}{M_{N_i}^2} \right] - \frac{m_{\zeta_I}^2}{m_{\zeta_I}^2 - M_{N_i}^2} \ln \left[\frac{m_{\zeta_I}^2}{M_{N_i}^2} \right] \right), \quad (9)$$

where U_{MNS} and m_ν are measured by neutrino oscillation experiments. And O is an arbitral complex 3 by 2 rotation matrix with $OO^T = \text{Diag}(0, 1, 1)$ ($O^T O = 1_{2 \times 2}$), which can be parametrized by the following matrices for the normal hierarchy (NH) and inverted hierarchy (IH) [18]:

$$O = \begin{bmatrix} 0 & 0 \\ \cos z & -\sin z \\ \pm \sin z & \pm \cos z \end{bmatrix}, \quad O = \begin{bmatrix} \cos z & -\sin z \\ \pm \sin z & \pm \cos z \\ 0 & 0 \end{bmatrix}, \quad (10)$$

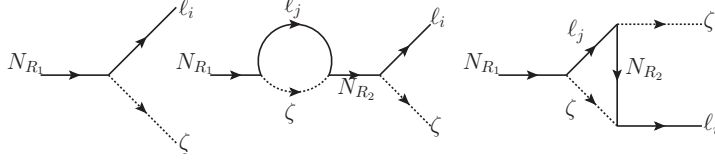


FIG. 2: Tree level and one-loop diagrams for $N_{R_1} \rightarrow l_i \zeta$.

respectively, where z can be complex. In our numerical analysis, we will use the global fit of the current neutrino oscillation data as the best fit values for NH and IH [19]:

$$\begin{aligned} \text{NH} : s_{12}^2 = 0.304, \quad s_{23}^2 = 0.452, \quad s_{13}^2 = 0.0218, \quad \delta_{CP} = \frac{306}{180}\pi, \\ (m_{\nu_1}, m_{\nu_2}, m_{\nu_3}) \approx (0, 8.66, 49.6) \text{ meV}, \end{aligned} \quad (11)$$

$$\begin{aligned} \text{IH} : s_{12}^2 = 0.304, \quad s_{23}^2 = 0.579, \quad s_{13}^2 = 0.0219, \quad \delta_{CP} = \frac{254}{180}\pi, \\ (m_{\nu_1}, m_{\nu_2}, m_{\nu_3}) \approx (49.5, 50.2, 0) \text{ meV}, \end{aligned} \quad (12)$$

where $s_{12,13,23}$ are the short-hand notations of $\sin \theta_{12,13,23}$ for three mixing angles of U_{MNS} , while two Majorana phases are taken to be zero.

B. Leptogenesis

Here, we discuss the resonant leptogenesis mechanism, followed by those in ref. [2].³ First of all, we expect that the source of the CP asymmetry (CPA) is induced from N_{R_1} via the two-body decay as shown in Fig. 2. Then, the CPA, which is denoted by ϵ , is approximately computed by

$$\epsilon \simeq -\frac{3}{16\pi} \frac{\text{Im} \left[(y_\zeta^\dagger y_\zeta)_{12}^2 \right]}{(y_\zeta^\dagger y_\zeta)_{11}} \frac{M_{N_1}}{M_{N_2}}, \quad (13)$$

where we have assumed $M_{N_1} \ll M_{N_2}$.⁴ During creating the lepton asymmetry, the decay width of N_{R_1} should satisfy the following condition of the out-of-equilibrium:

$$\Gamma(N_{R_1} \rightarrow \ell^\pm \zeta^\mp) \lesssim H(M_{N_1}), \quad (14)$$

³ A comprehensive study is found in, *e.g.*, ref. [20].

⁴ In our numerical analysis, we will take $3 \lesssim M_{N_1}/M_{N_2} \lesssim 10$ [21].

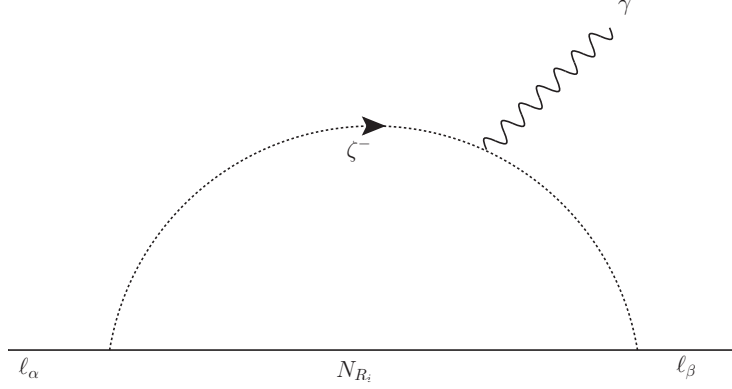


FIG. 3: One loop diagram for LFVs of $\ell_\alpha \rightarrow \ell_\beta \gamma$.

with

$$\Gamma(N_{R_1} \rightarrow \ell^\pm \zeta^\mp) = \frac{(y_\zeta^\dagger y_\zeta)_{11}}{16\pi} M_{N_1} \left(1 - \frac{m_{\zeta^\pm}^2}{M_{N_1}^2}\right)^2, \quad H(T) = \left(\frac{8\pi^3 g_*}{90}\right)^{1/2} \frac{T^2}{M_{Pl}}, \quad (15)$$

where $H(T)$ is the Hubble parameter at the temperature (T), $g_* \approx 100$ is the relativistic degrees of freedom, and $M_{Pl} \approx 10^{19}$ GeV is the Planck mass. Furthermore, one can derive the following condition:

$$(y_\zeta^\dagger y_\zeta)_{11} \lesssim \left(\frac{256\pi^5 g_*}{45}\right)^{1/2} \frac{M_{N_1}}{M_{Pl}} \left(1 - \frac{m_{\zeta^\pm}^2}{M_{N_1}^2}\right)^{-2}, \quad (16)$$

which implies $(1 - m_{\zeta^\pm}^2/M_{N_1}^2) = \mathcal{O}(10^{-5} \sim 10^{-4})$ for $y_\zeta = \mathcal{O}(10^{-3})$ and $M_{N_1} = \mathcal{O}(0.1 \sim 1)$ TeV, although we will numerically analyze later. Consequently, the resulting BAU (Y_B) is found as [21]

$$Y_B \simeq -\frac{1}{15} \frac{\epsilon}{g_*} = (5.8 \sim 6.6) \times 10^{-10}, \quad (17)$$

where the last value is the current bound on the BAU [22].

C. Lepton flavor violating processes

In our model, there exist various LFV processes such as $\ell_\alpha \rightarrow \ell_\beta \gamma$, $\ell_a \rightarrow \ell_b \ell_c \bar{\ell}_d$, and flavor changing processes involving quarks such as semi-leptonic decays. First of all, let us consider the processes $\ell_\alpha \rightarrow \ell_\beta \gamma$ in Fig. 3, which are induced from the neutrino Yukawa couplings at

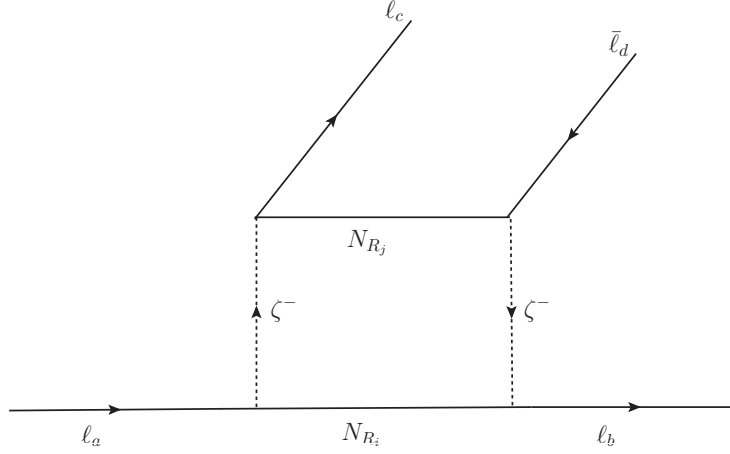


FIG. 4: Typical box diagrams for LFVs of $l_a \rightarrow l_b l_c \bar{l}_d$.

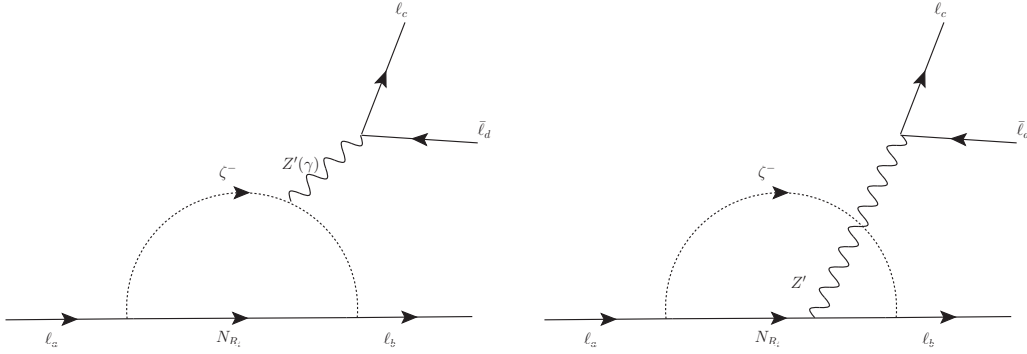


FIG. 5: One-loop diagrams via the $Z'(\gamma)$ boson for LFVs of $l_a \rightarrow l_b l_c \bar{l}_d$.

one-loop level. The decay branching ratios (BRs) are given by

$$\text{BR}(l_\alpha \rightarrow l_\beta \gamma) = \frac{3\alpha_{em} C_{\alpha\beta}}{16\pi G_F^2} \left| \sum_{i=1,2} \frac{(y_\zeta)_{\beta i} (y_\zeta^\dagger)_{i\alpha}}{M_{N_i}^2} F_I(r_{l_\alpha}, r_{N_i}) \right|^2, \quad (18)$$

$$F_I(r_{l_\alpha}, r_{N_i}) = \int_0^1 dx \int_0^{1-x} dy \frac{xy}{x + (1-x)r_{N_i} + (x^2-x)r_{l_\alpha}}, \quad (19)$$

where $r_{N_i} \equiv m_{\zeta^\pm}^2/M_{N_i}^2$, $r_{l_\alpha} \equiv m_{l_\alpha}^2/M_{N_i}^2$, $\alpha_{em} \approx 1/137$, $G_F \approx 1.17 \times 10^{-5} \text{ GeV}^{-2}$, $C_{\mu e} \approx 1$, $C_{\tau e} \approx 0.1784$, and $C_{\tau\mu} \approx 0.1736$. The simplified form in the limit of $r_{l_\alpha} \ll 1$ is read as

$$F_I(0, r_{N_i}) \approx \frac{2 + 3r_{N_i} - 6r_{N_i}^2 + r_{N_i}^3 + 6r_{N_i} \ln r_{N_i}}{(1 - r_{N_i})^4}. \quad (20)$$

Experimental upper bounds for the branching ratios of the LFV decays are found to be [23]:

$$\text{BR}(\mu \rightarrow e \gamma) \lesssim 4.2 \times 10^{-13}, \quad \text{BR}(\tau \rightarrow e \gamma) \lesssim 3.3 \times 10^{-8}, \quad \text{BR}(\tau \rightarrow \mu \gamma) \lesssim 4.4 \times 10^{-13}. \quad (21)$$

TABLE III: A summary of the constraints of three-body decay branching ratios (BRs).

Upper limits of BRs
$\text{BR}(\mu^- \rightarrow e^+ e^- e^-) \lesssim 1.0 \times 10^{-12}$
$\text{BR}(\tau^- \rightarrow e^+ e^- e^-) \lesssim 2.7 \times 10^{-8}$
$\text{BR}(\tau^- \rightarrow e^+ e^- \mu^-) \lesssim 1.8 \times 10^{-8}$
$\text{BR}(\tau^- \rightarrow e^+ \mu^- \mu^-) \lesssim 1.7 \times 10^{-8}$
$\text{BR}(\tau^- \rightarrow \mu^+ e^- e^-) \lesssim 1.5 \times 10^{-8}$
$\text{BR}(\tau^- \rightarrow \mu^+ e^- \mu^-) \lesssim 2.7 \times 10^{-8}$
$\text{BR}(\tau^- \rightarrow \mu^+ \mu^- \mu^-) \lesssim 2.1 \times 10^{-8}$

The stringent constraint comes from $\mu \rightarrow e\gamma$, and it roughly gives the upper limit $y_\zeta \lesssim \mathcal{O}(10^{-2})$ for $M_{N_1} = \mathcal{O}(100)$ GeV, where $M_{N_1} \ll M_{N_2}$ is expected from the leptogenesis.

Next, let us discuss the three-body LFV decays of $\ell_\alpha \rightarrow \ell_\beta \ell_c \bar{\ell}_d$. These decays are of course expected to be tiny compared to those of $\ell_\alpha \rightarrow \ell_\beta \gamma$ due to phase spaces as well as additional small couplings. In our case, they consist of two kinds of one-loop diagrams; box diagrams via Yukawa couplings in Fig. 4 and Penguin types of diagrams mediated by $\gamma(Z')$ boson via kinetic and Yukawa terms in Fig. 5. However since the diagram via γ is always smaller than the contributions of $\ell_\alpha \rightarrow \ell_\beta \gamma$ [24], it can be negligible. From the box diagrams in Fig. 4, the most stringent bound for the three-body decays arises from $\mu \rightarrow ee\bar{e}$ as shown in Table III, given by [22]

$$\text{BR}(\mu \rightarrow ee\bar{e}) \lesssim 1.0 \times 10^{-12}. \quad (22)$$

Here, we will estimate the theoretical bound in terms of the Yukawa coupling, by applying this experimental bound in Eq. (22). The bound on the Yukawa coupling for the box diagram in Fig. 4 is severely estimated as [26]

$$(y_\zeta)_{11}(y_\zeta)_{11}^\dagger \lesssim 8.6 \times 10^{-5} \frac{M_{N_1}}{\text{GeV}}. \quad (23)$$

Even when we take $M_{N_1} = \mathcal{O}(100)$ GeV that is the minimal mass allowed by leptogenesis, we find $(y_\zeta)_{11}(y_\zeta)_{11}^\dagger \lesssim \mathcal{O}(0.01)$; $\text{Min.}[y_\zeta] \simeq \mathcal{O}(0.1)$. This bound is weaker than the case of $\ell_\alpha \rightarrow \ell_\beta \gamma$ by one order of magnitude. From the Z' mediated diagrams in Fig. 5, one finds [26]

$$(y_\zeta)_{11}(y_\zeta)_{11}^\dagger \lesssim 2.62 \times 10^{-9} \left[\frac{m_{Z'}}{\text{GeV}} \right]^2 g'^{-2} \lesssim 0.13, \quad (24)$$

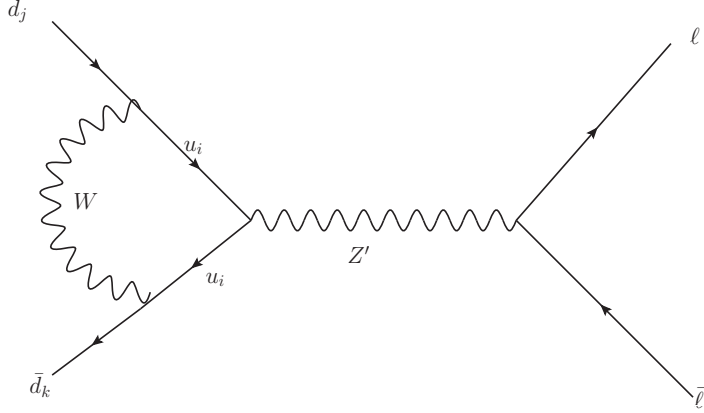


FIG. 6: Typical semi-leptonic decay mode.

where we have applied the relation $(g'/m_{Z'})^2 < (6.9 \text{ TeV})^{-2}$ given by the LEP experiment [25]. Clearly, Eq. (24) leads to $\text{Min.}[y_\zeta] \simeq \mathcal{O}(0.4)$, which is weaker than the box one.

Semi-leptonic decays also occur at one-loop level via the Z' boson in Fig. 6, where we neglect the contribution from the Yukawa coupling because it is tiny enough. The effective Hamiltonian is given by

$$\mathcal{H}_{\text{eff}} \approx -g_2^2 \sum_{i=u,c,t} \frac{(V_{\text{CKM}}^\dagger)_{ki}(V_{\text{CKM}})_{ij}F(u_i, W)}{(4\pi)^2} \left[\frac{g'}{m_{Z'}} \right]^2 (\bar{d}_k \gamma_\alpha P_L d_j)(\bar{\ell} \gamma^\alpha \ell), \quad (25)$$

where g_2 is the $SU(2)_L$ gauge coupling, V_{CKM} is the Cabibbo-Kobayashi-Maskawa mixing matrix, and $F(u_i, W)$ is an one-loop function that is order one at most. One of the stringent constraints comes from $\text{BR}(B_s \rightarrow \bar{\mu}\mu)$, and it is evaluated by the coefficient of the above effective Hamiltonian, given by

$$\text{BR}(B_s \rightarrow \bar{\mu}\mu) : \left| g_2^2 \sum_{i=u,c,t} \frac{(V_{\text{CKM}}^\dagger)_{si}(V_{\text{CKM}})_{ib}}{(4\pi)^2} \left[\frac{g'}{m_{Z'}} \right]^2 \right| \lesssim 5 \times 10^{-9} \text{ GeV}^{-2}, \quad (26)$$

where we have assumed $F(u_i, W) \approx 1$ and the right-hand side is the experimental bound of $\text{BR}(B_s \rightarrow \bar{\mu}\mu)$. As the numerical value of the left-hand side in Eq. (26) is the order 10^{-12} at most by applying the relation $(g'/m_{Z'})^2 < (6.9 \text{ TeV})^{-2}$, it is obviously within the experimental result.⁵ Thus, we will only consider the processes of $\ell_\alpha \rightarrow \ell_\beta \gamma$ in our numerical analysis below.

⁵ See ref. [16] for the other experimental bounds of semi-leptonic decays.

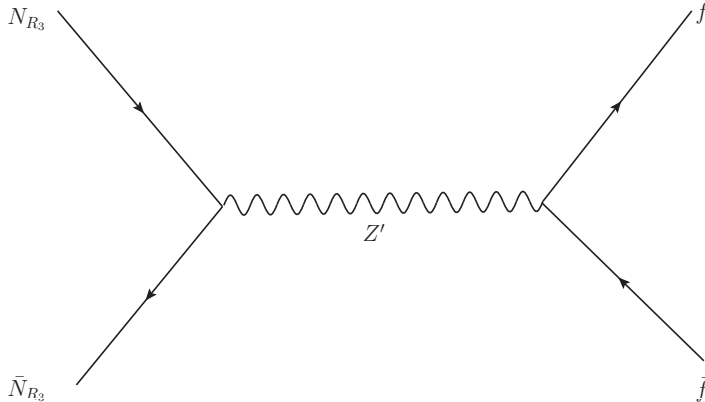


FIG. 7: Main contribution to induce the relic density of DM.

D. Dark matter

In our model, the possible DM candidates are $\zeta_{R/I}$ and the lightest one in $N_{R_{1,2,3}}$. For the scalar DM of $\zeta_{R/I}$, its nature is similar to the isospin doublet inert boson [27] except Yukawa and additional (gauged) boson interactions. However, since our typical scale of the Yukawa coupling y_ζ is around 10^{-3} , its modes cannot be dominant to explain the relic density of DM. Clearly, $\zeta_{R/I}$ cannot help to rely on the interactions of the Higgs potential and/or kinetic term. Nevertheless, it is known that there exist a lot of solutions to satisfy the present exclusion limits from the direct DM experimental detections, even when a model is minimal. To escape the limits from the spin independent direct detection searches reported by LUX [28], XENON1T [29], and PandaX-II [30], we have to consider two dominant modes from $Z^{(\prime)}$ and CP-even Higgs portals. The former one with the Z boson mediation can easily be evaded by giving the mass difference between ζ_R and ζ_I to be greater than $O(100)$ keV. Note that the constraint with the Z' mediation is always weaker than the Z one, since its cross section is proportional to $(g'/m_{Z'})^2 < (6.9 \text{ TeV})^{-2}$. The latter one can also be used to avoid the limits by taking the corresponding quartic Higgs couplings, which can be written in terms of linear combinations $\lambda_0, \lambda_{H\zeta}^{(\prime)}, \lambda_{\eta\zeta}^{(\prime)}, \lambda_{\zeta\varphi_{8(10)}}$, to be less than 0.01, when the SM Higgs is mediating and the other masses of CP-even Higgses are assumed to be heavier than the mass of the SM Higgs. As a summary of the bosonic DM candidate, one finds the solution at around 500 GeV of DM to satisfy the relic density of DM through the kinetic term. This is almost the same as the result of the DM model with one inert two-Higgs doublet [27].

In case of the fermion DM candidate such as the lightest state of $N_{R_{1,2,3}}$, its main modes to the relic density can be found in the kinetic term with the additional gauge boson, and/or the Higgs potential. As for both modes, its solution tends to be at around the pole with half masses of mediating fields. A comprehensive analysis has recently been done in refs. [6, 31, 32]. To satisfy the direct detection bounds, we have the similar processes from Z' and CP-even Higgses portals. With the same reason as the Z' mediation, there is almost no constraint. As a result, we should consider the CP-even Higgses only. The exclusion limits can be evaded by taking the corresponding quartic Higgs couplings of $y_{N_{i,3}} < 0.01$ [34]. Once we identify either of $N_{R_{1,2}}$ as DM, the allowed parameter space might be restricted a little ⁶. On the other hand, if N_{R_3} is DM, we can discuss the DM issue independently. Once the leptogenesis effect is taken into consideration, $N_{R_{1,2}}$ cannot be a DM candidate because of their appropriate decays. As a result, the reasonable DM candidate is N_{R_3} , and its dominant contribution is expected to be in the s-channel via the Z' boson in Fig. 7. The relic density of DM is formulated by [33]

$$\Omega h^2 \approx \frac{1.07 \times 10^9}{\sqrt{g_*(x_f)} M_{Pl} J(x_f) [\text{GeV}]}, \quad (27)$$

where x_f is assumed to be around 25, and $J(x_f) (\equiv \int_{x_f}^{\infty} dx \frac{\langle \sigma v_{\text{rel}} \rangle}{x^2})$ is evaluated by

$$J(x_f) = \int_{x_f}^{\infty} dx \left[\frac{\int_{4M_{N_3}^2}^{\infty} ds \sqrt{s - 4M_{N_3}^2} W(s) K_1 \left(\frac{\sqrt{s}}{M_{N_3}} x \right)}{16M_{N_3}^5 x [K_2(x)]^2} \right], \quad (28)$$

$$W(s) \approx \frac{25g'^4 (s - M_{N_3}^2)}{72\pi |s - m_{Z'}^2 + im_{Z'} \Gamma_{Z'}|^2} \left(2\sqrt{1 - \frac{4m_t^2}{s}} (2m_t^2 + s) + 131s \right), \quad (29)$$

$$\Gamma_{Z'} \approx \frac{13g'^2 m_{Z'}}{24\pi}, \quad (30)$$

with m_t the top quark mass. In Fig. 8, we show the relic density of DM as a function of M_{N_3} , where red(blue) line corresponds to $m_{Z'} = 350(700)$ GeV with $g' = 0.05$. As a trivial result, we find that the correct relic density can be obtained near the half-mass of Z' for each benchmark point.

⁶ Since the related Yukawa coupling y_ζ cannot be order one in order to lead the successful resonant leptogenesis, our final result does not change drastically.

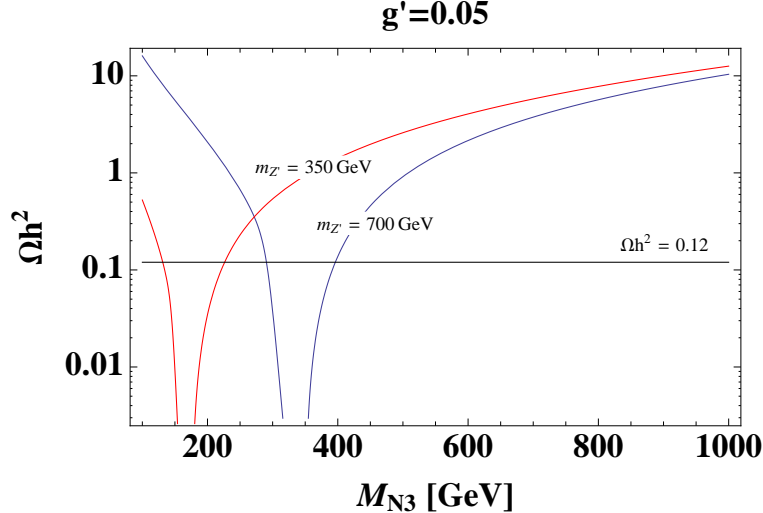


FIG. 8: The relic density of dark matter as a function of M_{N_3} , where red(blue) line corresponds to $m_{Z'} = 350(700)$ GeV with $g' = 0.05$.

III. NUMERICAL ANALYSIS

For the numerical calculations, we use the neutrino oscillation data in Eqs. (11) and (12) as well as the following input parameters:

$$\text{Re}[z] \in (0, \pi), \quad \text{Im}[z] \in (-10, -1), \quad (31)$$

$$(m_{\zeta_R}, M_{N_1}) \in (0.1, 10) \text{ TeV}, \quad M_{N_2} \in (3 \times M_{N_1}, 10 \times M_{N_1}) \text{ TeV}, \quad (32)$$

where we have taken $m_{\zeta_I} = m_{\zeta_{\pm}}$ to avoid the constraints from the oblique parameters [14], and $3 \lesssim M_{N_1}/M_{N_2} \lesssim 10$ [21] because the number density of N_{R_2} immediately decreases at the temperature below M_{N_2} .

Imposing the neutrino oscillation data, constraints from LFVs, and the BAU in Eq. (17) with the out-of-equilibrium condition in Eq. (16), we present our numerical analysis below. First of all, we show the benchmark point for several important values in the case of NH and IH in Table IV to easily confirm they satisfy experimental results as discussed above. In Fig. 9, we estimate the important value of $1 - m_{\zeta_+}^2/M_{N_1}^2$ to obtain a sizable BAU in terms of M_{N_1} for the cases of NH(left-side) and IH(right-side). When $M_{N_1} \lesssim 1$ TeV, $1 - m_{\zeta_+}^2/M_{N_1}^2 \lesssim 10^{-5}$ is required. Otherwise, the degeneracy between m_{ζ_+} and M_{N_1} becomes to be milder slightly. In Fig. 10, we show the scattering plots in the plane of $\text{BR}(\mu \rightarrow e\gamma)$ and M_{N_1} for NH and IH. We see that all values for whole the range of M_{N_1} are below the current

TABLE IV: Bench mark points (BPs) for several representative parameters of NH and IH.

	z	$(y_\zeta^\dagger y_\zeta)_{11}$	Y_B	$\text{Br}(\mu \rightarrow e\gamma)$	$\text{Br}(\tau \rightarrow e\gamma)$	$\text{Br}(\tau \rightarrow \mu\gamma)$	$\frac{m_{\zeta R}}{\text{TeV}}$	$\frac{m_{\zeta \pm}}{\text{TeV}}$	$\frac{M_{N_1}}{\text{TeV}}$	$\frac{M_{N_2}}{\text{TeV}}$
NH	2.8-8.2 <i>i</i>	2.7×10^{-5}	6.0×10^{-10}	6.2×10^{-20}	1.0×10^{-22}	4.7×10^{-22}	0.20	1.3	1.3	7.0
IH	1.4-9.0 <i>i</i>	3.2×10^{-5}	6.0×10^{-10}	3.1×10^{-22}	2.2×10^{-25}	1.5×10^{-25}	0.81	7.7	7.7	6.4

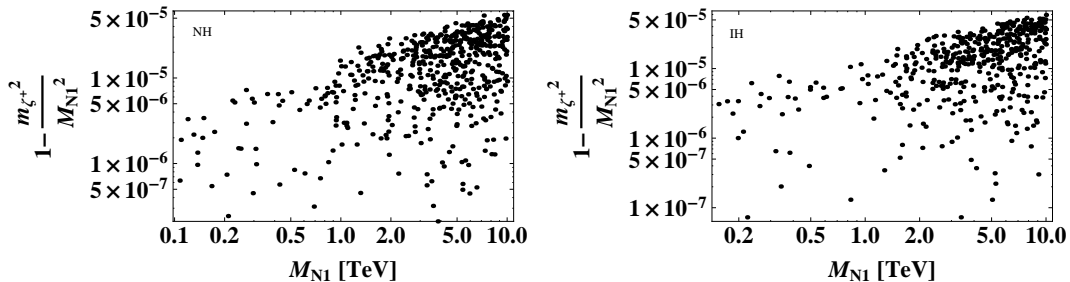


FIG. 9: Scattering plots to satisfy all the data in the plane of M_{N_1} and $1 - m_{\zeta+}^2 / M_{N_1}^2$, where the left and right figures correspond to NH and IH, respectively.

experimental bound. This is the trivial consequence in order to get the sizable BAU via leptogenesis. In Fig. 11, we display the plots of $y_{\zeta_{11}} - y_{\zeta_{12}}$ for NH and IH, where we separate $y_{\zeta_{11}} - y_{\zeta_{12}}$ into the real and imaginary parts. These figures suggest that the IH case is greater than the NH one by a few times. In Fig. 12, we illustrate the plots of $y_{\zeta_{31}} - y_{\zeta_{32}}$ similar to Fig. 11. These figures indicate that the NH case is slightly greater than the IH one, opposite to Fig. 11.

IV. CONCLUSION

We have proposed a radiatively generated neutrino mass model with a successful leptogenesis to produce the BAU at TeV scale, which contains a gauged $U(1)_{B-L}$ symmetry with unusual charge assignments of $(-4, -4, 5)$ to the right-handed neutrinos. In this model, DM candidates naturally arrive without imposing any additional symmetry to stabilize DM, which is achieved by the resulting symmetry after the SSB of $U(1)_{B-L}$. We have examined the allowed regions for the model parameters to satisfy all the experimental constraints. We

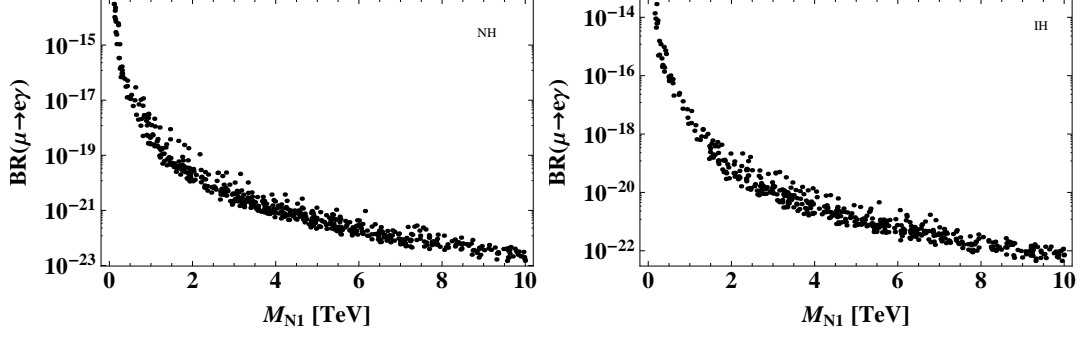


FIG. 10: Scattering plots to satisfy all the data in the plane of $\text{BR}(\mu \rightarrow e\gamma)$ and M_{N_1} , where the left and right figures correspond to NH and IH, respectively.

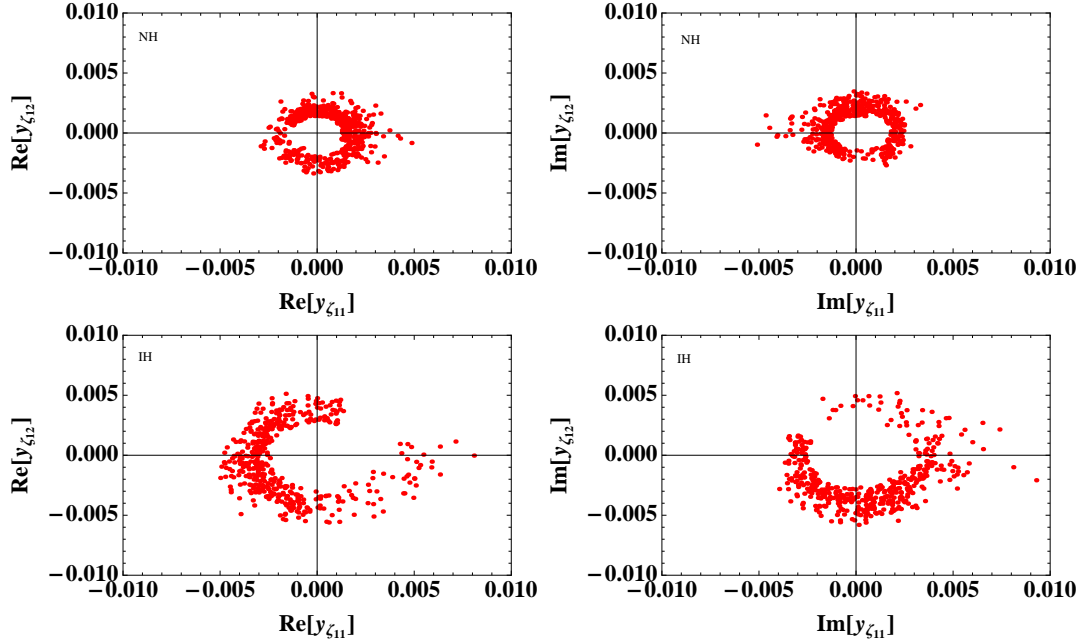


FIG. 11: Scattering plots to satisfy all the data in the planes of $\text{Re}[y_{\zeta_{11}}] - \text{Re}[y_{\zeta_{12}}]$ (left-side) and $\text{Im}[y_{\zeta_{11}}] - \text{Im}[y_{\zeta_{12}}]$ (right-side), where the top (bottom) figure represents NH (IH).

have found that the Yukawa couplings $y_{\zeta_{\alpha\beta}}$ with a typical order of 10^{-3} lead to small LFV processes, which cannot be measured at the current experiments.

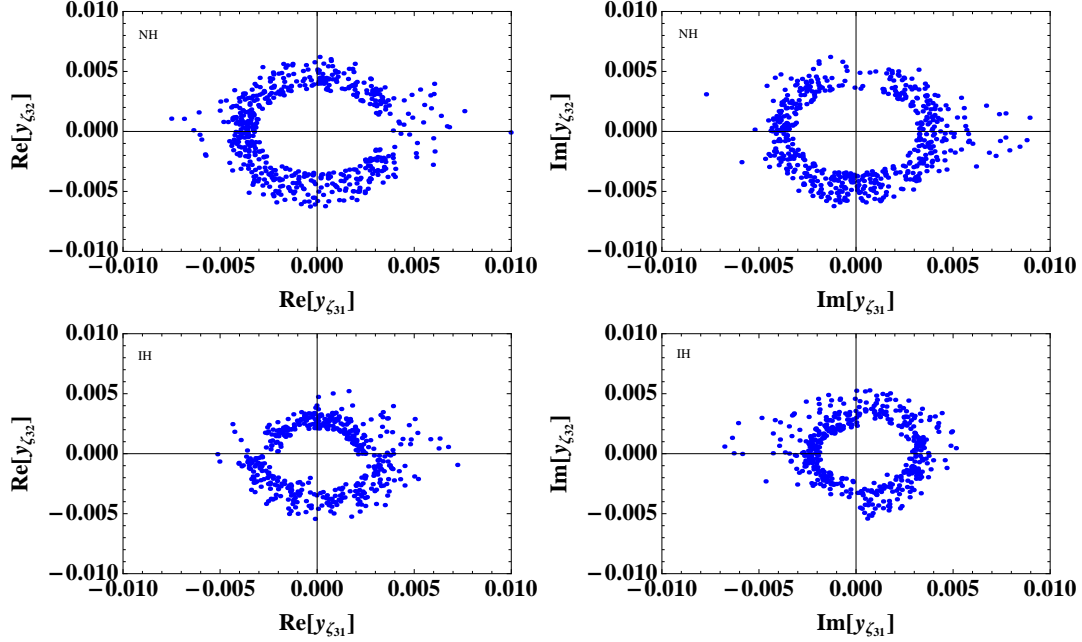


FIG. 12: Scattering plots to satisfy all the data in the planes of $\text{Re}[y_{\zeta_{31}}] - \text{Re}[y_{\zeta_{32}}]$ (left-side) and $\text{Im}[y_{\zeta_{31}}] - \text{Im}[y_{\zeta_{32}}]$ (right-side), where the top (bottom) figure represents NH (IH).

Acknowledgments

This work was supported in part by National Center for Theoretical Sciences and MoST (MoST-104-2112-M-007-003-MY3).

-
- [1] E. Ma, Phys. Rev. D **73**, 077301 (2006).
 - [2] C. H. Chen, C. Q. Geng and D. V. Zhuridov, JCAP **0910**, 001 (2009).
 - [3] J. Chang *et al.* [ATIC Collaboration], Nature **456**, 362 (2008); O. Adriani *et al.* [PAMELA Collaboration], Nature **458**, 607 (2009); A. A. Abdo *et al.* [Fermi LAT Collaboration], Phys. Rev. Lett. **102**, 181101 (2009).
 - [4] J. C. Montero and V. Pleitez, Phys. Lett. B **675**, 64 (2009).
 - [5] S. Patra, W. Rodejohann and C. E. Yaguna, JHEP **1609**, 076 (2016).
 - [6] T. Nomura and H. Okada, arXiv:1705.08309 [hep-ph].
 - [7] T. Nomura and H. Okada, arXiv:1708.08737 [hep-ph].
 - [8] D. Nanda and D. Borah, arXiv:1709.08417 [hep-ph].

- [9] V. De Romeri, E. Fernandez-Martinez, J. Gehrlein, P. A. N. Machado and V. Niro, arXiv:1707.08606 [hep-ph].
- [10] T. Appelquist and R. Shrock, Phys. Rev. Lett. **90**, 201801 (2003) doi:10.1103/PhysRevLett.90.201801 [hep-ph/0301108].
- [11] T. Appelquist and R. Shrock, Phys. Lett. B **548**, 204 (2002) doi:10.1016/S0370-2693(02)02854-X [hep-ph/0204141].
- [12] C. Q. Geng and R. E. Marshak, Phys. Rev. D **39**, 693 (1989).
- [13] J. F. Gunion, H. E. Haber, G. L. Kane and S. Dawson, “The Higgs Hunter’s Guide,” Front. Phys. **80**, 1 (2000).
- [14] R. Barbieri, L. J. Hall and V. S. Rychkov, Phys. Rev. D **74**, 015007 (2006).
- [15] S. Schael *et al.* [ALEPH and DELPHI and L3 and OPAL and LEP Electroweak Collaborations], Phys. Rept. **532**, 119 (2013).
- [16] M. Carpentier and S. Davidson, Eur. Phys. J. C **70**, 1071 (2010) doi:10.1140/epjc/s10052-010-1482-4 [arXiv:1008.0280 [hep-ph]].
- [17] J. A. Casas and A. Ibarra, Nucl. Phys. B **618**, 171 (2001).
- [18] T. Rink and K. Schmitz, JHEP **1703**, 158 (2017).
- [19] M. C. Gonzalez-Garcia, M. Maltoni and T. Schwetz, JHEP **1411**, 052 (2014).
- [20] J. Heeck and D. Teresi, Phys. Rev. D **94**, no. 9, 095024 (2016) doi:10.1103/PhysRevD.94.095024 [arXiv:1609.03594 [hep-ph]].
- [21] P. H. Gu and U. Sarkar, Mod. Phys. Lett. A **25**, 501 (2010).
- [22] C. Patrignani *et al.* [Particle Data Group], Chin. Phys. C **40**, 100001 (2016).
- [23] A. M. Baldini *et al.* [MEG Collaboration], Eur. Phys. J. C **76**, no. 8, 434 (2016).
- [24] T. Toma and A. Vicente, JHEP **1401**, 160 (2014) doi:10.1007/JHEP01(2014)160 [arXiv:1312.2840 [hep-ph]].
- [25] S. Schael *et al.* [ALEPH and DELPHI and L3 and OPAL and LEP Electroweak Collaborations], Phys. Rept. **532**, 119 (2013). doi:10.1016/j.physrep.2013.07.004 [arXiv:1302.3415 [hep-ex]].
- [26] A. Crivellin, S. Najjari and J. Rosiek, JHEP **1404**, 167 (2014) doi:10.1007/JHEP04(2014)167 [arXiv:1312.0634 [hep-ph]].
- [27] T. Hambye, F.-S. Ling, L. Lopez Honorez and J. Rocher, JHEP **0907**, 090 (2009); Erratum: [JHEP **1005**, 066 (2010)].

- [28] D. S. Akerib *et al.* [LUX Collaboration], Phys. Rev. Lett. **118**, no. 2, 021303 (2017).
- [29] E. Aprile *et al.* [XENON Collaboration], arXiv:1705.06655 [astro-ph.CO], recently accepted by Phys. Rev. Lett..
- [30] X. Cui *et al.* [PandaX-II Collaboration], arXiv:1708.06917 [astro-ph.CO], recently accepted by Phys. Rev. Lett..
- [31] S. Singirala, R. Mohanta and S. Patra, arXiv:1704.01107 [hep-ph].
- [32] S. Singirala, R. Mohanta, S. Patra and S. Rao, arXiv:1710.05775 [hep-ph].
- [33] J. Edsjo and P. Gondolo, Phys. Rev. D **56**, 1879 (1997) doi:10.1103/PhysRevD.56.1879 [hep-ph/9704361].
- [34] S. Kanemura, S. Matsumoto, T. Nabeshima and N. Okada, Phys. Rev. D **82**, 055026 (2010) doi:10.1103/PhysRevD.82.055026 [arXiv:1005.5651 [hep-ph]].